Monitoring of the freezing stage in a freeze-drying process using IR thermography

International Journal of Pharmaceutics [ISSN: 0378-5173], 566, 488-499. DOI: 10.1016/j.ijpharm.2019.06.005

Monitoring of the freezing stage in a freeze-drying process using IR thermography

Domenico Colucci, Riccardo Maniaci, Davide Fissore*

Dipartimento di Scienza Applicata e Tecnologia, Politecnico di Torino,

Corso Duca degli Abruzzi 24, 10129 Torino, Italy

* *Corresponding author*

email: davide.fissore@polito.it

tel: 0039-011-0904693

Abstract

This paper presents a new Process Analytical Technology based on the use of an infrared camera and a mathematical model to estimate the ice crystal size distribution obtained at the end of the freezing stage of a vial freeze-drying process. Both empirical laws and first-principle based equations, already presented in the Literature, may be used to this purpose, if the temperature gradient in the frozen product and the freezing front rate are obtained from the analysis of the thermal images. The resistance of the dried product to vapor flux may be then calculated from the distribution of the ice crystal diameters, thus enabling the use of a one-dimensional model for process simulation and optimization. Freeze-drying of 5% and 10% w/w aqueous sucrose solutions, and of 5% w/w aqueous mannitol solutions, were considered as case study. The results were validated comparing the calculated diameters of the pores of the dried cake, corresponding to the ice crystal diameters, with the results experimentally obtained from the analysis of the SEM images, and comparing the values of drying duration and maximum product temperature calculated with the mathematical model with those measured experimentally. Results evidences the effectiveness of the proposed system for process monitoring.

Keyword

Freeze-drying, freezing, crystal size, monitoring, IR camera, Process Analytical Technology.

1. Introduction

Freeze-drying is a key step in the manufacturing process of several pharmaceutical and biopharmaceutical products formulated as liquid solutions. In fact, it allows extending the shelf life of the formulation being processed through the removal of the water at low temperature, without jeopardizing heat-labile molecules like the active pharmaceutical ingredients. The process encompasses three steps (see, among the others, Mellor, 1978; Jennings, 1999; Oetjen and Haseley, 2004; Fissore, 2013):

- Freezing, when most of the water (the "free water") turns from the liquid into the solid state;
- Primary drying, when the ice is removed through sublimation, at low temperature and pressure;
- Secondary drying, when the water not frozen in the first stage (the "bound water") is removed through desorption, at low pressure and higher temperature with respect to that of the primary drying.

While in the freezing stage it is necessary to remove heat from the product, thus decreasing its temperature and promoting the water crystallization, in the drying stages it is required to supply heat to the product, as both sublimation and desorption are endothermic processes.

The freeze-drying process is surely much "gentler" towards the products than other drying processes requiring higher operating temperatures. Nevertheless, product quality may be compromised at the end of the process if the operating conditions of the drying stages, namely the temperature of the heating shelf and the pressure in the drying chamber, are not carefully selected. In particular, product temperature has to remain below a threshold value, that is a characteristic of the formulation being processed, to avoid the collapse of the dried product (in case of amorphous formulations) or its melting (for crystalline products) (Pikal et

al., 1990a, 1990b; Fissore, 2013). This is particularly true for the primary drying stage, where the limit temperature is lower, due to the higher amount of water in the product; besides, this stage can be really long-lasting, thus making process optimization a real need.

The freezing phase plays a fundamental role within the freeze-drying process as it determines the structure of the product (Hottot et al., 2007). In fact, if the dried product does not collapse (and this is the main goal of every freeze-drying processes), the diameter of the ice crystals coincides with the size of the pores formed in the dried product. Larger pores result in a lower resistance to water vapor flow from the interface of sublimation to the dying chamber, and, therefore, accelerate the primary drying process (Searles et al., 2001). Vice versa, the desorption rate of the secondary drying stage is penalized by the reduction of the specific surface that occurs in the presence of high pore diameters (Oddone et al., 2017). The morphology of the product is therefore of fundamental importance for the efficiency of the lyophilization process and on the quality of the product. In fact, small-sized pores make it possible to reach high temperatures during primary drying and, therefore, make the undesirable excess of the collapse temperature easier. This is due to the fact that product temperature is the result of a heat balance between the heat transferred to the product and that removed through sublimation: in case of small sized pores the sublimation rate is lowered and, thus, also the heat removed from the product, thus making possible to reach higher temperatures. Moreover, in the case of products sensitive to interfacial denaturation, such as proteins, the formation of small ice crystals considerably increases the phenomena of unfolding and aggregation (Bhatnagar et al. 2008). Finally, the morphology of the product also significantly influences the reconstitution time of highly concentrated formulations, and this can have critical effects in some applications (Geidobler et al., 2013).

The ice crystal distribution obtained at the end of the freezing stage can be determined using various techniques. As an example, scanning electron microscopy (SEM) can be

combined with image analysis techniques to determine pore size distribution in lyophilized products (Grassini et al., 2016, Arsiccio et al., 2019). The SEM technique allows the determination of the heterogeneity in the pore size within the tested vial and can be used off-line. This represents an advantage, as the introduction of additional sensors inside the freeze dryer is not required. Another technique that can be used off-line is the BET (Brunauer – Emmett – Teller) analysis, which allows measuring the surface area of the freeze-dried product and, from the latter, to trace back the pore size (Rambhatla et al., 2004). Finally, micro-computerized X-ray tomography (X-ray micro-CT) can be used to determine the pore size distribution within the product (Pisano et al., 2017).

As an alternative, it is possible to use predictive approaches, based on the application of mathematical models or empirical laws, that allow the determination of the pore diameters in the lyophilized product starting from the knowledge of some process variables. The advantage of these techniques is that they may be used in-line and may, thus, be exploited for the real time design and optimization of the primary drying stage. This paper is focused on this second group of methods, whose application generally requires knowing the evolution of the temperature gradient in the product already frozen, as well as the advancement rate of the freezing interface.

An innovative system, based on non-contact temperature measurement through an IR camera, is used in this paper to get the process variables required to estimate the size of the ice crystals. Moreover, these values are used to infer one of the key parameters of the one-dimensional mathematical model frequently used for process design and optimization, namely the resistance of the dried cake to vapor flux. By this way, it becomes possible, at the end of the freezing stage, to estimate both drying time and product temperature during the following primary drying stage for a given set of operating conditions and, if desired, to optimize the process. At the best of the authors knowledge no other work addressed the possibility of a real time estimation of the product structure and optimization of the freeze-drying cycle without any

need to model the heat and mass transfer phenomena occurring during the whole freezing stage.

The paper is organized as follows: at first the methods for crystal size estimation and the application of the IR camera to estimate the variables of interest, the main novelty of this study, are presented. Then, the mathematical models of the primary drying stage are briefly reviewed and that used in this paper is described in detail, and the case studies investigated for validation purposes are described. Results are then presented and discussed, and the main conclusions of the study are finally presented.

2. Materials and methods

2.1 Crystal size estimation

Empirical models were proposed in the Literature to allow estimating the size of the crystals at the end of a solidification process. Bald (1991) proposed the following equation:

$$d_p = \alpha \left(\frac{dT}{dt} \right)^{-\beta} \tag{1}$$

where the crystal size is assumed to be proportional to the rate of temperature change in the system, being α and β determined by comparing calculated and measured crystal size. Other equations proposed in the literature consider the velocity of the solidification front, *R*, and the temperature gradient in the frozen product, *G*:

$$d_p = aR^{-\lambda_1} G^{-\lambda_2} \tag{2}$$

where *a*, λ_1 and λ_2 have to be determined experimentally. Equation (2) was used to model the solidification of metal samples at low rates (Kurz and Fisher, 1992), apples (Bomben and King, 1982), starch gels (Reid, 1984), alloys at high rate (Kochs et al., 1991), gelatine (Woinet, 1998), and also the freezing of aqueous solutions in vials (Nakagawa et al., 2007; Bosca et al., 2015, 2017; Pisano and Capozzi, 2017). In the latter case *R* and *G* are calculated as follows:

$$R(t) = \frac{dL_{frozen}(t)}{dt} \tag{3}$$

$$G(t) = \frac{T_f - T_B(t)}{L_{frozen}(t)} \tag{4}$$

and may change, obviously, with time. With respect to the parameters a, λ_1 and λ_2, Nakagawa et al. (2007), as well as Bosca et al. (2015, 2017) and Pisano and Capozzi (2017), used $\lambda_1 = \lambda_2 = 0.5$, and the parameter a was obtained looking to the ice crystal sizes distribution obtained experimentally to get the best fit between calculated and measured values of ice crystal size.

Arsiccio et al. (2017) proposed a first-principle based model for calculating d_p from R and G, based on a heat balance of the crystal growth phase, once nucleation has occurred. In case of dilute solutions, their equation, where again R and G appear, reads:

$$d_p = \frac{4\varepsilon\gamma b R}{\left(\varepsilon\rho_{frozen} R\Delta H_f - k_{frozen} G\right) G^{2/3}} \tag{5}$$

In this case the unknown parameter is γb, i.e. the product of the solid-solid interface tension (γ) and of a parameter b that has to be determined experimentally.

Regardless of the equation used to calculate the ice crystal diameter, it has to be pointed out that both R and G are needed, and they were usually obtained off-line from the mathematical simulation of the process. Complex multiphase simulation (Nakagawa et al., 2007) or simplified iterative algorithms (Arsiccio et al. 2018) were proposed to get the evolution of product temperature along the axial positions of the sample during the freezing stage, as well as the position of the freezing front.

In this work a different method, based on thermal monitoring with IR camera, is used to get R and G, as it will be described in the following.The empirical equation (2), referred to as model #1 in the following, and equation (5), referred to as model #2, will be used to calculate d_p. With model #1 we used $\lambda_1 = \lambda_2 = 0.5$ and $a = 4.59$ μm $s^{-0.5}$ $K^{0.5}$ for sucrose solutions (Bosca

et al., 2015) while a = 1.7 μm $s^{-0.5}$ $K^{0.5}$ was used for mannitol solutions (Napoletano, 2016). With model #2, values of γb were taken from Arsiccio et al. (2017), i.e. γb = 230000 J $K^{(2/3)}$ $m^{(-8/3)}$ for sucrose solutions and γb = 70000 J $K^{(2/3)}$ $m^{(-8/3)}$ for mannitol solutions.

2.2 IR camera and temperature measurement

The measurement of the evolution of product temperature in the freezing stage is crucial to estimate the diameter of the ice crystals. The product temperature can be measured using thermocouples, placing the sensor inside one or more vials of the batch, but they allow measuring the temperature just in a specific point of the system, without providing any information about the temperature gradient in the frozen product (G), and about the freezing front rate (R) (Schneid and Gieseler, 2008; Bosca et al., 2013a, Nail et al., 2017; Fissore et al., 2018). Besides, it is well known that they may affect the nucleation of the ice crystals, by reducing the supercooling degree, thus making the monitored vial not representative of the whole batch, although their effect in lab-scale units, where the process is carried out in non-GMP conditions, is less relevant (Bosca et al., 2013b). As an alternative, optical fibers, with the fiber Bragg gratings embedded in the shelf, were investigated (Kasper et al., 2013), but they are not able to solve the problem of obtaining G and R. Moreover, alternative configurations were proposed, e.g. optical fibers were formed to the shape of a helix, placed inside the vial to allow measuring the product temperature in several positions, but this could affect, up to some extent, the behavior of the product in the freezing stage. Less invasive systems were also proposed, e.g. the possibility of embedding T-type thermocouples with a thickness ranging from 50 to 200 nm into the glass wall (Parvis et al., 2012, 2014; Grassini et al., 2013), but they are able just to partially solve the problem of getting the values of G and R *vs*. time.

Emteborg et al. (2014) firstly proposed using infrared (IR) camera to monitor product temperature in a freeze-drying process. In their system there is no contact between the sensor

and the product, but the camera is placed outside the chamber, being installed on the top, thus monitoring only the temperature of the top surface of the product in the top shelf. Van Bockstal et al. (2018) used an IR camera to monitor a new continuous freeze-drying process, being able to track product temperature along the glass vial wall. Lietta et al. (2019) designed a system that can be placed inside the chamber, standing in front of several vials, thus able to follow the evolution of the axial temperature profile during the whole process, as well as to monitor several vials at the same time, thus accounting for the batch intrinsic non-uniformity (Barresi et al., 2010).

In this work the same sensor described and validated by Lietta et al. (2019) was used to measure the temperature evolution of the product during the freezing stage. The system includes a FLIR thermal camera (model A35), a HDTV RGB camera (not used in this study), and a microprocessor where data are stored. These elements are placed in a protective enclosure (IMC Services s.r.l., Italy) realized with a thermally insulating plastic material. The role of the container is to protect the electronics of the system from the low temperature, low pressure and high moisture that characterize the drying chamber, while being transparent to WiFi communications, in order to allow data transfer from the microprocessor to the computer external to the freeze-drier.

Before using this device for temperature mapping, the emissivity of the glass vial was measured using the ISO 18434-1 (International Standard ISO, 2008) guideline (Part 1, Annex A.2). For a temperature of -30°C, the mean emissivity calculated was 0.95, while a value of 0.935 was obtained at -20°C and of 0.915 at 0°C.

As the IR camera measures the temperature of the glass wall, the measured value has to be corrected aiming to infer the temperature of the product inside the vial. The procedure proposed by Van Bockstal et al. (2018) was used to this purpose. Figure 1 shows an example of the results obtained in a freezing run, comparing the product temperature measured through

a thermocouple inserted in one vial of the batch, in close contact with the bottom of the vial, and the measurement of the IR camera, in the same position, corrected using the algorithm of Van Bockstal et al. (2018), pointing out the great accuracy of the IR based system. In any case, it must be highlighted that the difference between the external glass temperature, directly measured by the IR camera, and product temperature, measured by the thermocouple, is very low, about 0.2°C.

The main advantage of an IR camera with respect to a thermocouple is that product temperature is measured in the whole product. If it is straightforward to obtain a measurement of the axial temperature profiles, that is the gradients across the product, and from the analysis of the evolution of the temperature distribution inside the product it is also possible to measure the rate of movement of the freezing front. Since both nucleation and crystal growth are exothermic phenomena, the axial position of the freezing front can be detected as a maximum of temperature. After image pre-processing, namely the correction of the optical aberration induced by the lens, object identification and segmentation, to remove from the analysis everything apart from the product inside the monitored vials, three axial temperature profiles were extracted for each vial (in central position and at the edges of the vial) and averaged, see Figure 2A. Averaging three measurements of the same variables helps to get rid of part of the noise that is typical of this kind of measurements without any real loss of information. In every image the local maximum was detected and tracked over time (in Figure 2A the position of this maximum is presented as a white triangle). The difference of the temperature measured in the position highlighted as the actual moving freezing front and that obtained at the bottom of the vial (see an example of these curves in Figure 2B) provides also the required information for the estimation of G, the temperature gradient inside the frozen layer. In Figure 2C an example of the evolution of the maximum temperature position along the whole cooling and freezing process is reported. The position of the maximum temperature is reported as the nondimensional

ratio between the actual pixel position where the maximum temperature was detected and the total height of the product (in pixels). During cooling, the maximum temperature, initially positioned somewhere around the center of the product, moves toward the top, and here remains until nucleation occurs. When nucleation occurs it suddenly moves to the bottom of the vial and it moves back to the top. This part of the trajectory was sampled to show the evolution, in different instants of time, of the freezing front. The difference in the positions obtained between a certain number of consecutive frames, the symbols shown in Figure 2C, divided by the time occurring between these measurements, provides the value of *R*. The great amount of noise at the end of the trajectory tells about an almost flat profile with local maxima varying with time: freezing is completed, and the system is moving towards the thermal equilibrium with the environment.

It has to be pointed out that in our study we considered to monitor 10 vials per batch, evaluating the averages of the monitored variables, and reporting results as average values and ranges of variation. Here we are in fact presenting a proof of concept and for this purpose we considered ten vials to be enough. However, a higher number of vials could be considered: the maximum number of vials that is possible to monitor depends on the actual sensor and field of view. The algorithm presented can provide the same results for each and every one of the vials visualized: it is the User choice to take into account the differences between the different vials and/or extract an average value.

2.3 Mathematical modelling and estimation of the resistance of the dried product to vapor flux

As it has been pointed out in the Introduction section, primary drying is the most critical stage of the whole freeze-drying process. Mathematical modelling can strongly support the design of the process, allowing the *in silico* simulation of the primary drying stage, and both off-line (Giordano et al., 2011; Fissore et al., 2011a; Koganti et al., 2011) or in-line (Daraoui et al.,

2010; Pisano et al., 2010, 2011a) optimization of the process. It is obviously necessary to use a model that accurately describes the evolution of the system, and quite often a mono-dimensional model represents an optimal compromise between accuracy and complexity (Velardi and Barresi, 2008). In this framework, the heat flux to the product (J_q) and the mass flux from the interface of sublimation to the drying chamber (J_w) are given by the following equations:

$$J_q = K_v \left(T_{shelf} - T_B \right) \tag{6}$$

$$J_w = \frac{1}{R_p} \left(p_{w,i} - p_{w,c} \right) \tag{7}$$

where T_{shelf} is the heating shelf temperature, T_B is the product temperature at the bottom of the vial, $p_{w,i}$ is the water partial pressure at the sublimation interface (that can be calculated using one of the equations appeared in the Literature and relating it to the temperature, see the review of Fissore et al., 2011b), and $p_{w,c}$ is water partial pressure in the drying chamber (usually assumed to be equal to total chamber pressure, being the composition of the gas in the chamber about 100% water vapor).

Once the values of J_w and J_q are known, the following equations may be written:

$$J_q = \Delta H_s J_w \tag{8}$$

$$\frac{dL_{frozen}}{dt} = -\frac{1}{\rho_{frozen} - \rho_{dried}} J_w \tag{9}$$

corresponding to the heat balance at the sublimation interface (eq. (8)) and to the mass balance for the frozen product (eq. (9)). A further equation is needed to relate the temperature of the product at the interface of sublimation (T_i), that is needed to calculate $p_{w,i}$, to the temperature of the product at the bottom of the vial (T_B):

$$T_B = T_{shelf} - \frac{1}{K_v} \left(\frac{1}{K_v} + \frac{L_{frozen}}{k_{frozen}} \right)^{-1} \left(T_{shelf} - T_i \right) \tag{10}$$

Equation (10) is obtained from the energy balance of the frozen product, where heat

accumulation is neglected (as a consequence of the slow rate of the process).

The solution of model equations (6)-(10) requires to know the value of the parameters K_v and R_p. K_v is the overall heat transfer coefficient, that may be accurately estimated by the gravimetric test (Pisano et al., 2011b) without consuming any product, as the test may be carried out filling the same kind of vials used for the freeze-drying process just with water. The coefficient K_v is just a function of the vial-freeze dryer system and can be estimated independently from the product being processed.

The estimation of R_p is more challenging, as it is a function of the type of product being processed, of the freezing conditions and, also, of the thickness of the dried product:

$$R_p = R_{p,0} + \frac{AL_{dried}}{1 + BL_{dried}} \tag{11}$$

Several ways were proposed in the literature to estimate in line R_p, for a given product. Fissore et al. (2017) proposed to use the temperature measurement directly obtained through a thermocouple placed in the vial, while Bosca et al. (2013b) used the temperature measurement coupled with a mathematical model, thus obtaining a soft-sensor, to get this parameter. Unfortunately, the presence of the thermocouple could affect the nucleation of the ice crystals and, thus, up to some extent, the structure of the dried product, in particular when the process is carried out in GMP (Good Manufacturing Practice) conditions, where the accuracy of the results obtained by this way may be not as high as required. As an alternative, TDLAS (Tunable Diode Laser Absorption Spectroscopy) sensor may be used to estimate a mean value of R_p (Kuu et al., 2011), but this requires a retrofitting of the dryer to place the sensor in the duct connecting the chamber to the condenser, and this may be hardly feasible (in some cases even impossible). Also the pressure rise test may be used to this purpose (Fissore et al., 2011b), but, again, the test may affect product dynamics (and in industrial practice this test is usually carried out only at the end of the primary drying stage, to check that ice sublimation is effectively completed).

In this paper we propose to use the information about the ice crystal diameters obtained

from monitoring the freezing stage to get R_p. In fact, in the primary drying stage the empty spaces through which the vapor flows correspond to the ice crystals that disappeared. Since the vapor flux in the dried cake occurs in Knudsen regime (the Knudsen number is typically greater than 3) (Ho and Roseman, 1979; Fissore and Pisano, 2015), it is possible to write:

$$J_w = D_e \frac{c_{w,i} - c_{w,c}}{L_{dried}} \tag{12}$$

and, using the ideal gas law:

$$J_w = \frac{M_w D_e}{R_g T} \frac{p_{w,i} - p_{w,c}}{L_{dried}} \tag{13}$$

Therefore, considering eq. (7), it comes that:

$$R_p = \frac{R_g T_i}{M_w D_e} L_{dried} \tag{14}$$

The temperature T appearing in eq. (13) has been replaced with T_i in eq. (14) as the temperature in the dried product usually ranges in a small interval of values and, thus, the percentage effect of the gradient of temperature on R_p is very low, and a constant value may be assumed. The effective diffusivity may be related to the Knudsen diffusivity (D_k) through the following equation:

$$D_e = \frac{\varepsilon}{\tau} D_k \tag{15}$$

where D_k is related to pore size and temperature by means of the following equation (Ho and Roseman, 1979):

$$D_k = K \frac{d_p}{2} T_i^{0.5} \tag{16}$$

being K a constant parameter equal to 22.9 m/s $K^{0.5}$. Substituting eq. (16) into eq. (15) we get:

$$D_e = \frac{d_p}{2\tau} K \varepsilon T_i^{0.5} \tag{17}$$

and, after substituting eq. (17), eq. (14) reads:

$$R_p = \frac{R_g T_i^{0.5}}{M_w \frac{d_p}{2\tau} K\varepsilon} L_{dried} \quad (18)$$

Equation (18) can be used to estimate R_p as a function of L_{dried} once the values of d_p vs. L_{dried} are known. As previously shown, the axial distribution of d_p may be estimated at the end of the freezing stage since, provided that no shrinkage or collapse occurs, the size of the pores corresponds to that of the ice crystals.

2.4 Case study

Experiments were carried out in a pilot-scale freeze-dryer (LyoBeta, Testar, Spain). The drying chamber has a volume of 0.2 m^3, and the total area of the four shelves is 0.5 m^2. The system is equipped with:

- Thin T-type thermocouples (Tersid, Italy), that can be placed in some of the vials of the batch, to provide additional temperature measurements;
- A capacitance (Baratron type 626A, MKS Instruments, USA) and a thermal conductivity (Pirani type PSG-101-S, Inficon, Switzerland) manometer, used for pressure monitoring.

The ratio of the two pressure signals is used to identify the ending point of the primary drying stage (Patel et al., 2010).

Tests were carried out using sucrose solutions, either 5% or 10% by weight, and mannitol solutions, 5% by weight. Reactants were purchased from Sigma Aldrich (≥99.5%) and used as received. Solutions were prepared with ultra-pure water produced using a Millipore water system (Milli-Q RG, Millipore, Billerica, MA). After preparation, solutions were poured into ISO 8362-1 10R glass vials (Schott Pharmaceutical Packaging, Inc., Lebanon, USA), directly loaded onto the shelf of the drying chamber and partially stoppered with an igloo stopper (NovaPure Chlorobutyl Igloo Stoppers, West Pharma, Exton, USA).

Shelf-ramped freezing (Kasper and Friess, 2011) was used in the freezing-stage as it is the most extensively applied freezing method in pharmaceutical companies. According to this method the temperature of the product, placed on the shelves contained in the drying chamber, is gradually reduced because of the decrease of the temperature of the fluid flowing inside the shelves. In this study the set point of the shelf temperature was always set to -50°C, resulting in a cooling rate of the technical fluid equal to about -1.5°C/min from room temperature till about -10°C, then about -0.5°C/min from -10°C to -30°C and, finally, about -0.3°C/min from -30°C to -50°C.

No controlled nucleation was used in the freezing step since uncontrolled nucleation, which still represents the standard in industrial freeze-drying, does not jeopardize the accuracy of the results obtained.

Beside the freezing tests, in some cases also primary drying was carried out, aiming to compare the experimental duration of the process with that calculated by using the mathematical model of the process and the parameters estimated in the freezing stage. Moreover, completely dried samples could be analyzed by scanning electron microscopy (SEM), aiming to compare the pores size distribution with that estimated from the ice crystal distribution. In this case primary drying was carried out at 10 Pa, with a shelf temperature of -20°C for the sucrose-based solutions, while for the mannitol solutions the shelf temperature was increased to -10°C. In this case 30 vials were loaded in the drying chamber, arranged according to a hexagonal array, while for the freezing tests just 4 vials, placed in front of the IR camera, were loaded in the chamber.

After drying, the product in the two vials right in front of the camera of every batch were analyzed with a scanning electron microscope (SEM, FEI type, Quanta Inspect 200, Eindhoven, The Netherlands). Firstly, samples were fixed on aluminium circular stubs, and metallized with chrome. Images were taken, for each sample, along the total thickness of the product,

considering three different radial positions, i.e. in the center of the samples and at the edges, where the product was in contact with the glass wall. By this way it was possible to adequately account for the within-vial non-uniformity of the cake structure.

The SEM images of the porous product structure obtained are 1024 x 768 pixels and were segmented, using Multivariate Image Analysis (MIA) techniques (Prats-Montalbán et al., 2011), to estimate the axial pore distribution inside the product. Figure 3A reports one of these images. SEM images can frequently present a non-uniform brightness due to the so-called *charging effect*, that is some regions of the picture are on average lighter than other. Following the approach of Grassini et al. (2016) a moving average filter (low-pass filter equalization) with dimension 256 pixels x 256 pixels was used.

Following the approach proposed by Bharati and MacGregor (2000), the images were first pretreated to obtain the so called "Bharati matrix", a data structure that accounts for both the information of the intensity of the single pixel and the textural information. A PCA model is a linear decomposition of a data structure $\mathbf{X}(I \times J)$:

$$\mathbf{X} = \mathbf{T} \cdot \mathbf{P}^{\mathrm{T}} + \mathbf{E} \tag{19}$$

where $\mathbf{T}$ is the $I \times A$ score matrix, $\mathbf{P}$ is the $J \times N$ loading matrix and $\mathbf{E}$ is the residual matrix, having the same dimension of the original matrix $\mathbf{X}$. N is the number of principal components extracted, I the number of pixels extracted from the image to build the Bharati structure and J equals nine as the number of pixels of the 3x3 moving window used to build the Bharati structure. Since all the values of the Bharati matrix were pixel intensities no further data pretreatments were performed.

A Principal Component Analysis (PCA) model (Pearson, 1901, Hotelling, 1933), with one single latent variable, was extracted from this data structure. This first latent variable is basically related to the information on the average intensity of the single pixels, neglecting any information about the gradients typically related to the presence of borders, fractures and texture

in general. The segmentation of the pores was achieved removing all the pixel with a score lower than a certain threshold, arbitrarily fixed. The result was a logical image where the segmented regions were represented as areas of "1" and all the rest was set to zero.

To make sure that all the thin borders between two adjacent pores were removed, avoiding the detection of pores with an overestimated global area, a second mask was created segmenting both the white regions of the picture and those characterized by strong intensity gradients. Simple image analysis techniques were used to this purpose (Gonzalez et al., 2004) like the "Canny" algorithm for edges detections (Canny, 1986). The obtained image was subtracted, pixel by pixel, from the one previously obtained. Subtraction between logical matrices corresponds to take the logical OR of each corresponding couple of pixels. Before counting the number of pores and estimate area, perimeter and equivalent diameter for each one of them, one further dimensional filter was applied to remove all the regions having an area lower than 50 or greater than one hundred thousand pixels. If the former can hardly be discriminated from the noise, the latter usually correspond to fractures or micro-collapses inside the product that will have the only real effect of skewing to the right the resulting pore distribution. Figure 3B presents a qualitative result of the segmentation of image 3A. The pixels of the original grey-scale image corresponding to the segmented areas of the resulting segmented image were colored in white. The white spots are the pores segmented: even if they are all pictured in the same color, the single pores could be clearly distinguished. For each image the histogram of the pore diameters was created and 5^{th}, 25^{th}, 50^{th}, 75^{th} and 95^{th} percentiles were calculated. The results obtained from the selected vials were averaged.

3. Results and discussion

The system proposed in this study is based on (i) thermal imaging, to get the values of the

freezing from rate (R) and of the temperature gradient in the frozen product (G) in the freezing stage (G), and on an equation relating R and G to the ice crystal diameters. Both the empirical law expressed by eq. (2) (model #1) and the first-principle based eq. (5) (model #2) were used. Figure 4 shows the estimated pore diameters obtained for the 5% w/w sucrose solution using model #1, Figure 4A or model #2, Figure 4B. The range of variation of each value of ice crystal diameter, represented as error bar in each graph, corresponds to one standard deviation in the value of d_p. In fact, in each freezing test four values of R and G were available, one for each monitored vial, and each test was repeated 9 times, thus allowing the calculation of mean value and standard deviation for the crystal diameters. It has to be remarked that no preliminary experiments were carried out for parameters tuning, as the parameters of the model equations, namely a for model #1 and γb for model #2, were taken from the literature. The trend of the two curves of d_p vs. L_{frozen} is the same: lower values of crystal size are obtained at the bottom of the vial, because of the higher temperature gradients, related to the high cooling rate, and at the top of the vial, as a result of the solute concentration occurring in the freezing stage. Larger ice crystals were forecast in the middle. Slightly different values of ice crystal diameters were obtained, for the same axial position, depending on the model used, with slightly lower values in case model #1 is used. At the bottom and at the top of the frozen product the values of d_p estimated with model #1 and with model #2 are very similar, around 50 μm, being the largest difference in the central position, where d_p values close to 70 μm and 120 μm are estimated from model #1 and model #2 respectively. We could have fit a new set of model parameters, namely a for model #1 and γb for model #2, able to provide perfectly overlapping curves of d_p vs. L_{frozen} and, indeed, in good agreement with the experimentally measured ones. Since the scope of this work is to develop a *ready-to-use* Process Analytical Technology (PAT) and test it, not to discuss the performances of the models already presented, we used the parameters available in Literature. Furthermore, the final aim of this work is not the precise estimation of

the pore diameters, but the correct prediction of the maximum temperature experienced by the product and the ending point of the primary drying stage and, thus, we must investigate the effect of this uncertainty on these target variables.

Results obtained for the 10% w/w sucrose solution, using both model #1 and #2, are given in Figure 5. Both curves show a similar trend, with higher values of d_p in the central position estimated by model #2. In this case also at the top and at the bottom of the sample model #2 provides higher values of d_p with respect to model #1. When considering the range of variability of each value of d_p, as for the data shown in Figure 4, it appears that the two curves are partially overlapping.

For the 5% w/w aqueous mannitol solution the trend of the curves of d_p vs. L_{frozen} was similar to that of the sucrose-based solution, but with, obviously, different values. In this case, as shown in Figure 6, it appears that very close curves of mean d_p vs. L_{frozen} were obtained using model #1 and model #2 with Literature parameters.

Validation of these results was carried out in two steps: (i) comparing the calculated diameters of the ice crystals, corresponding to the pores of the dried cake, with those measured through SEM analysis of the dried product, and (ii) comparing the values of drying duration and maximum product temperature calculated with the mathematical model whose parameter R_p is obtained from the estimated values of d_p with those measured experimentally. Figure 7 shows the experimentally measured values of d_p, as a function of the axial position, for both the 5% and the 10% w/w sucrose solution. In this case the range of variability is given as the 25^{th} and the 75^{th} percentiles. These values are compared with the mean values calculated using model #1 and model #2 (shown in Figures 4 and 5), without reporting the range of variability for clarity purposes.

The agreement between calculated and measured variables is considered to be acceptable: this is due to the fact that the mean calculated value of d_p at a certain value of L_{frozen}

falls in the range of pore diameters measured experimentally. When evaluating results shown in Figure 7 it has in fact to be taken into account both the uncertainty related to samples preparation for SEM analysis, and the uncertainty related to the image analysis, and also the range of variation of the values of d_p at a certain value of L_{frozen} calculated from the temperature gradients obtained through IR camera. Moreover, we are interested in the prediction of the product temperature and drying duration in the primary drying and as long as the estimates of d_p, that means the values of R_p calculated, allows an accurate estimate of the target variables, as it will be shown in the following, then the accuracy of the estimates may be considered acceptable.

Once the curve of d_p vs. L_{frozen} has been estimated we can infer the curve of R_p vs. L_{dried} using the approach previously described, thus obtaining, with the *in silico* simulation of the process, the values of drying duration and of maximum product temperature for a given couple of values of shelf temperature and chamber pressure. This allows verifying, for example, if the product will remain in the design space for the selected operating conditions of the following primary drying, or if any change in these operating conditions is required. The first step is thus to estimate the curve of R_p vs. L_{dried}. Figure 8 reports examples of the resulting curves of R_p vs. L_{dried} for the 5% w/w (upper graph) and the 10% w/w (lower graph) sucrose solutions, using model #1 or model #2 to calculate the ice crystal size. As it could be expected slightly lower values of cake resistance are obtained, for a given thickness of the dried product, when using model #2 for estimating the ice crystal size. In fact, as shown in Figures 4 and 5, the size of the ice crystals estimated by model #2 is slightly higher and this turns into a lower resistance of the dried product in the primary drying stage.

Beside the curve of R_p vs. L_{dried} it is necessary to calculate the value of K_v for the vial freeze-dryer system under investigation. This test must be carried out just once, and it does not require to fill the vials with the (frequently expensive and sometimes unavailable) active

pharmaceutical ingredient. For the system under investigation a value of 28 $Wm^{-2}K^{-1}$ was obtained with a gravimetric test carried out at the same pressure of the freeze-drying cycles.

Figure 9 shows the comparison between the calculated evolution of the frozen layer thickness in case of the 5% w/w (upper graph) and of the 10% w/w (lower graph) sucrose solutions using the R_p values obtained through model #1. Drying time is the time instant when L_{frozen} goes to zero, here compared, for validation purposes, with the pressure ratio curves. The actual moment the primary drying ends is one of most desired and difficult parameters to estimate in a vacuum freeze-drying process, taking also into account the non-uniformity of the batch. It appears to depend on the kind of sugar and its structure and is not possible, even using the state-of-the-art methodology for its evaluation, to write down a single value to be compared with the result obtained from a single simulation using a simplified 1D model of the process. The onset and offset values of the pressure ratio curve have been reported together with the actual value simulated to make sure the reader understands our simulation falls inside the best experimental estimation that could be provided that is the time lapse going from the onset to the offset. The 5% b.w. sucrose solution was simulated to be completely dried in 28.95 h, while in Figure 9B the L_{frozen} goes to zero in 27.33 h. In both cases the drying time falls in the range identified by the onsets (23.53 h and 25.36 h respectively) and offsets (35.89 h for the 5% b.w. solution and 30.33 h for the 10% b.w. one) of the pressure ratio curves, very close to the offset, where drying process is usually considered to be completed (Patel et al., 2010). With respect to the maximum product temperature, for the 5% w/w sucrose solution a value of -33°C was experimentally obtained, while for the 10% sucrose solution the maximum measured temperature was -32°C. The calculated maximum product temperature was -31.7°C for the 5% w/w sucrose solution and -30.7°C for the 10% w/w sucrose solution, with an error of 1.3°C.

Better results were obtained using the first-principle based model (#2). Results are shown in Figure 10 for both the 5% w/w and the 10% w/w sucrose solutions. As a consequence

of the lower values of the dried cake resistance calculated (see Figure 8), the calculated drying time is slightly lower (26.03 h the former and 24.6 h the latter), but, again, in the range identified by the onset and offset of the pressure ratio curves. With respect to the maximum product temperature values, -33.2°C and -32.5°C are the values obtained, respectively, for the 5% w/w and the 10% w/w sucrose solutions, thus resulting in an error of 0.2°C and 0.5°C respectively.

Regarding the test involving the mannitol solution, the maximum product temperature measured was -20°C, while a value of -20.6°C was calculated using the values of R_p obtained through model #1, and a value of -21.5°C was obtained with the values of R_p obtained through model #2. In both cases, the comparison between the curves of L_{frozen} vs. time and that of the pressure ratios resulted in conclusions similar to those presented for the sucrose-based solutions.

Looking at both case studies, namely sucrose and mannitol-based solutions, no univocal indication of the best approach (model #1 or model #2) can be inferred: while the estimated values of drying duration are in all cases acceptable, more accurate estimates of maximum product temperature are obtained using model #2 for sucrose-based solutions, and using model #1 for mannitol-based solutions. In any case, it has to be highlighted that for both formulations the estimated values of maximum product temperature, whatever the model used, is, considering the uncertainty of the measurements, in agreement with the experimental values.

4. Conclusions and future perspectives

The potential of IR thermography for freeze-drying monitoring are well established for the primary drying stage: it is a unique system able to measure product temperature not just in a single point, and without any interference with the product. This paper has explored the application of IR thermography to the freezing stage: a simple algorithm has been proposed to

identify the freezing front and track its evolution as well as that of the temperature gradient in the frozen product. Using these two variables and either an empirical or a first-principle based equation it is then possible to estimate the size of the ice crystals and, thus, the resistance of the dried product to vapor flow. No mathematical modelling or time-consuming simulations of the freezing stage are required, allowing a real time evaluation of the resulting product structure. If the heat transfer coefficient to the product in the vial is somehow known, then it is possible to infer, before the starting of the primary drying, both the maximum temperature of the product and the duration of this stage. By this way it is possible to check if the product will remain inside the design space and, if not, check for other values of the operating conditions. In this sense, the presented PAT could be used to discriminate a successful batch from one that will present issues of any kind during the drying and should be rejected. Future work will prove the methodology here described for the purpose.

Whatever the model used, the accuracy of the estimates obtained for the maximum temperature of the product and the drying time falls within the uncertainty range of the experimental measurements, thus highlighting its potential for freeze-drying practitioners.

The validation of the system has been carried out considering sucrose-based and mannitol-based solutions, without any active pharmaceutical ingredient (API). In fact, freezing of a pharmaceutical solution is a crystallization from fuse process and the thermal evolution of the product is the result of the heat removed by the cooling medium and the heat released during the ice crystals nucleation and growth. The rationale for this work, and many other like this one, is that tracking and modelling this thermal evolution we can infer the pore distribution. In a pharmaceutical solution the API is present in a very low amount: the thermal properties of the solution can hardly be dependent on the API, that is the reason why, given the cost of the most common APIs, they are usually neglected, at least at the beginning, when a proof of concept of a PAT has to be tested. Nevertheless, even if the API was able to affect the thermal evolution

of the process, either the maximum temperature in the axial profile appears in different positions or moves at a different speed, the system is able to track that difference and provide different values of R and G, thus different crystal sizes. Absolutely different is the case where the API affects, given the same thermal evolution, the actual pore distribution. Given the really low concentrations, we expect the API might only mildly influence the kinetics of nucleation and crystal growth, although Koop et al. (2000) claimed that the solute does not affects the nucleation kinetics. The main consequence of this is that the equations relating R and G to ice crystals diameters (eqs. (2) or (5)) are no longer correct and different models should be used. Therefore, in case the system is used to monitor a process with a solute for which the validity of eqs. (2) or (5) has not been yet verified, and, thus, the parameters a and γb are unknown, a preliminary study to assess the freezing model and parameters has to be carried out, but this is evidently beyond the scope of this study and, in any case, for the above mentioned reasons, is expected to be required only in very few cases.

Future developments of the work will prove the effectiveness of the proposed PAT also in case of different cooling strategies, or when a controlled nucleation protocol is applied. The possible application of an image analysis-based algorithm to the real time monitoring of a continuous freezing process will also be investigated.

Acknowledgements

The contribution of Maitê Harguindeguy (Politecnico di Torino) to the experimental investigation, and that of Roberto Pisano, Sabrina Grassini and Leonardo Iannucci (Politecnico di Torino) to sample preparation and analysis of the dried products through SEM is gratefully acknowledged.

List of Symbols

A	parameter used to express the dependence of R_p on L_{dried}, s^{-1}
a	parameter used to calculate the size of the ice crystals as a function of R and G, μm K $m^{-0.5}$ $s^{-0.5}$
B	parameter used to express the dependence of R_p on L_{dried}, m^{-1}
b	coefficient of eq. (5), $K^{2/3}$ $m^{-2/3}$
$c_{w,c}$	water vapor concentration in the drying chamber, mol m^{-3}
$c_{w,i}$	water vapor concentration at the interface of sublimation, mol m^{-3}
D_e	effective diffusivity, m^2 s^{-1}
D_k	Knudsen diffusivity, m^2 s^{-1}
d_p	diameter of the ice crystals, m
E	residual matrix
G	temperature gradient in the frozen product, K m^{-1}
ΔH_f	heat of crystallization, J kg^{-1}
ΔH_s	heat of sublimation, J kg^{-1}
I	number of pixels extracted from the image to build the Bharati structure
J	number of pixels of the moving window used to build the Bharati structure
J_q	heat flux to the product, W m^{-2}
J_w	mass flux, kg $s^{-1}m^{-2}$
K	parameter used in eq. (16), m $s^{-1}K^{-0.5}$
K_v	overall heat transfer coefficient between the heating fluid and the product at the vial bottom, W $m^{-2}K^{-1}$
k_{frozen}	thermal conductivity of the frozen layer, W m^{-1} K^{-1}
L_{dried}	thickness of the dried product, m

L_{frozen}	thickness of the dried product, m
M_w	water molecular weight, kg mol^{-1}
N	number of principal components
P	loading matrix
$P_{Baratron}$	pressure measured by a capacitance (Baratron) gauge, Pa
P_{Pirani}	pressure measured by a thermal conductivity (Pirani) gauge, Pa
$p_{w,c}$	water vapor partial pressure in the drying chamber, Pa
$p_{w,i}$	water vapor partial pressure at the interface of sublimation, Pa
R	freezing front rate, K m^{-1}
R_g	ideal gas constant, J mol^{-1} K^{-1}
R_p	resistance of the dried product to vapour flux, Pa m^2 s kg^{-1}
$R_{p,0}$	parameter used to express the dependence of R_p on L_{dried}, m s^{-1}
T	score matrix
T_B	product temperature at the vial bottom, K
T_f	freezing temperature of the product, K
T_i	temperature of the product at the interface of sublimation, K
T_{shelf}	heating shelf temperature, K
T	temperature, K
t	time, s
X	data matrix

Greeks

α	parameter used in eq. (1), m s K^{-1}
β	parameter used in eq. (1), -
γ	solid-solid interfacial tension, J m^{-2}

ε	porosity of the dried product, -
λ_1	parameter used to express the dependence of d_p on R, -
λ_2	parameter used to express the dependence of d_p on G, -
τ	tortuosity of the dried product, -
ρ_{dried}	apparent density of the dried product, kg m^{-3}
ρ_{frozen}	density of the frozen product, kg m^{-3}

List of References

Arsiccio, A., Barresi, A.A., Pisano R., 2017. Prediction of ice crystal size distribution after freezing of pharmaceutical solutions. Cryst. Growth Des. 17(9), 4573-4581. https://doi.org/10.1021/acs.cgd.7b00319

Arsiccio, A., Barresi, A.A., De Beer, T., Oddone, I., Van Bockstal, P.J., Pisano R., 2018. Vacuum induced surface freezing as an effective method for improved inter- and intra-vial product homogeneity. Eur. J. Pharm. Biopharm. 128, 201-219. https://doi.org/10.1016/j.ejpb.2018.04.002

Arsiccio, A., Sparavigna, A.C., Pisano, R., Barresi, A.A., 2019. Measuring and predicting pore size distribution of freeze-dried solutions. Drying Technol., 37(4), 435-447. https://doi.org/10.1080/07373937.2018.1430042

Bald, W.B., 1991. Ice crystal growth in idealised freezing system, in Bald, W.B. (Ed.), Food Freezing, 1st edition. Springer-Verlag, London, UK, pp. 67–80 (Chapter 5).

Barresi, A.A., Pisano, R., Rasetto, V., Fissore, D., Marchisio, D.L., 2010. Model-based monitoring and control of industrial freeze-drying processes: effect of batch non-uniformity. Drying Technol. 28(5), 577-590. https://doi.org/10.1080/07373931003787934

Bharati, M.H., MacGregor, J.F., 2000. Texture analysis of images using Principal Component Analysis. Proceeding of SPIE/Photonics Conference on Process Imaging for Automatic Control, Boston, pp 27-37.

Bhatnagar, B.S., Pikal, M.J., Robin, H.B., 2008. Study of the individual contributions of ice formation and freeze-concentration on isothermal stability of lactate dehydrogenase during freezing. J. Pharm. Sci. 97(2), 798-814. https://doi.org/10.1002/jps.21017

Bomben, J.L., King, C.J., 1982. Heat and mass transport in the freezing of apple tissue. Int. J. Food Sci. Technol. 17(5), 615–632. https://doi.org/10.1111/j.1365-2621.1982.tb00221.x

Bosca, S., Corbellini, S., Barresi, A. A., Fissore D., 2013a. Freeze-drying monitoring using a new process analytical technology: Toward a “zero defect” process. Drying Technol. 31(15), 1744–1755. https://doi.org/10.1080/07373937.2013.807431

Bosca S., Barresi A. A., Fissore D., 2013b. Use of a soft-sensor for the fast estimation of dried cake resistance during a freeze-drying cycle. Int. J. Pharm. 451(1-2), 23-33. https://doi.org/10.1016/j.ijpharm.2013.04.046

Bosca, S., Barresi, A.A., Fissore, D., 2015. Design of a robust soft-sensor to monitor in-line a freeze-drying process. Drying Technol. 33(9), 1039-1050. https://doi.org/10.1080/07373937.2014.982250

Bosca, S., Barresi, A.A., Fissore, D., 2017. On the robustness of the soft sensors used to monitor a vial freeze-drying process. Drying Technol. 35(9), 1085-1097, https://doi.org/10.1080/07373937.2016.1243553

Canny, J., 1986. A Computational Approach to Edge Detection. IEEE Trans. Pattern Anal. Mach. Intell. 8(6), 679-698.

Daraoui, N., Dufour, P., Hammouri, H., Hottot, A., 2010. Model predictive control during the primary drying stage of lyophilisation. Contr. Eng. Pract. 18(5), 483-494. https://doi.org/10.1016/j.conengprac.2010.01.005

Emteborg, H., Zeleny, R., Charoud-Got, J., Martos, G., Luddeke, J., Schellin, H., Teipel K., 2014. Infrared thermography for monitoring of freeze-drying processes: Instrumental developements and preliminary results. J. Pharm. Sci. 103(7), 2088-2097. https://doi.org/10.1002/jps.24017

Fissore, D., 2013. Freeze drying of pharmaceuticals, in Swarbrick, J. (Ed.), Encyclopedia of Pharmaceutical Science and Technology, 4th edition, volume III. Taylor and Francis, New York, pp. 1723-1737. https://doi.org/10.1081/E-EPT4-120050278

Fissore, D., Pisano R., 2015. Computer-aided framework for the design of freeze-drying cycles: Optimization of the operating conditions of the primary drying stage. Processes 3(2), 406-421.

https://doi.org/10.3390/pr3020406

Fissore, D., Pisano, R., Barresi, A.A., 2011a. Advanced approach to build the design space for the primary drying of a pharmaceutical freeze-drying process. J. Pharm. Sci. 100(11), 4922-4933. https://doi.org/10.1002/jps.22668

Fissore, D., Pisano, R., Barresi, A.A., 2011b. On the methods based on the Pressure Rise Test for monitoring a freeze-drying process. Drying Technol 29(1), 73-90. https://doi.org/10.1080/07373937.2010.482715

Fissore, D., Pisano, R., Barresi, A.A., 2017. On the use of temperature measurement to monitor a freeze-drying cycle for pharmaceuticals. Proceedings of IEEE International Instrumentation and Measurements Technology Conference (I2MTC), Torino, Italia, May 22–25, paper 17039633, 1276-1281. https://doi.org/10.1109/I2MTC.2017.7969890

Fissore, D., Pisano, R., Barresi A.A., 2018. Process analytical technology for monitoring pharmaceuticals freeze-drying – A comprehensive review. Drying Technol. 36(15), 1839-1865. https://doi.org/10.1080/07373937.2018.1440590

Geidobler, R., Konrad, I., Winter, G., 2013. Can controlled ice nucleation improve freeze-drying of highly-concentrated protein formulations? J. Pharm. Sci. 102(11), 3915-3919. https://doi.org/10.1002/jps.23704

Giordano, A., Barresi, A.A., Fissore, D., 2011. On the use of mathematical models to build the design space for the primary drying phase of a pharmaceutical lyophilization process. J. Pharm. Sci. 100(1), 311-324. https://doi.org/10.1002/jps.22264

Gonzalez, R.C., Woods, R.E., Eddins S.L., 2004. Digital image processing using Matlab. Pearson education, Inc., Upper Saddle River, New Jersey.

Grassini, S., Parvis, M., Barresi A.A., 2013. Inert thermocouple with nanometric thickness for lyophilization monitoring. IEEE Trans. Instrum. Meas. 62(5), 1276–1283. https://doi.org/10.1109/TIM.2012.2223312

Grassini, S., Pisano, R., Barresi, A.A., Angelini, E., Parvis, M., 2016. Frequency domain image analysis for the characterization of porous products. Measurement, 94, 515–522. https://doi.org/10.1016/j.measurement.2016.08.031

Ho, N.F.H., Roseman, T.J., 1979. Lyophilization of pharmaceutical injections: Theoretical physical model. J. Pharm. Sci. 68,1170–1174. https://doi.org/10.1002/jps.2600680930

Hotelling, H., 1933. Analysis of a complex of statistical variables into principal components. J. Educ. Psychol., 24, 417–441. https://doi.org/10.1037/h0071325

Hottot, A., Vessot, S., Andrieu, J., 2007. Freeze-drying of pharmaceuticals in vials: Influence of freezing protocol and sample configuration on ice morphology and freeze-dried cake texture. Chem. Eng. Process. 46(7), 666-674. https://doi.org/10.1080/07373930600626388

International Standard ISO 18434-1, 2008. Condition monitoring and diagnostics of machines - Thermography - Part 1: General procedures. https://www.iso.org/obp/ui/#iso:std:iso:18434:-1:ed-1:v1:en (last access date: April 2019)

Jennings, T.A., 1999. Lyophilization: introduction and basic principles. Interpharm/CRC Press, Boca Raton.

Kasper, J.C., Wiggenhorn, M., Resch, M., Friess W., 2013. Implementation and evaluation of an optical fiber system as novel process monitoring tool during lyophilization. Eur. J. Pharm. Biopharm. 83(3), 449-459. https://doi.org/10.1016/j.ejpb.2012.10.009

Kasper, J.C., Friess W., 2011. The freezing step in lyophilization: physico-chemical fundamentals, freezing methods and consequences on process performance and quality attributes of biopharmaceuticals. Eur. J. Pharm. Biopharm. 78(2), 248-263. https://doi.org/10.1016/j.ejpb.2011.03.010

Kochs, M., Korber, C.H., Heschel, I., Nunner, B., 1991. The influence of the freezing process on vapour transport during sublimation in vacuum freeze-drying. Int. J. Food Sci. Technol. 34(9), 2395-2408. https://doi.org/10.1016/0017-9310(91)90064-L

Koganti, V.R., Shalaev, E.Y., Berry, M.R., Osterberg, T., Youssef, M., Hiebert, D.N., Kanka, F.A., Nolan, M., Barrett, R., Scalzo, G., Fitzpatrick, G., Fitzgibbon, N., Luthra, S., Zhang, L., 2011. Investigation of design space for freeze-drying: Use of modeling for primary drying segment of a freeze-drying cycle. AAPS PharmSciTech 12(3), 854-861. https://doi.org/10.1208/s12249-011-9645-7

Koop, T., Luo, B., Tsias, A., Peter, T., 2000. Water activity as the determinant for homogeneous ice nucleation in aqueous solutions. Nature, 406, 611-614.

Kurz, W., Fisher D.J., 1992. Fundamentals of Solidification, Trans Tech Publications, Switzerland.

Kuu, W.Y., O'Bryan, K.R., Hardwick, L.M., Paul, T.W., 2011. Product mass transfer resistance directly determined during freeze-drying cycle runs using tunable diode laser absorption spectroscopy (TDLAS) and pore diffusion model. Pharm. Dev. Tech. 16(4), 343-357. https://doi.org/10.3109/10837451003739263

Lietta, E., Colucci, D., Distefano, G., Fissore D., 2019. On the use of infrared thermography for monitoring a vial freeze-drying process. J. Pharm. Sci. 108(1), 391-398. https://doi.org/10.1016/j.xphs.2018.07.025

Mellor, J.D., 1978. Fundamentals of freeze-drying. Academic Press, London.

Nail, S., Tchessalov, S., Shalaev, E., Ganguly, A., Renzi, E., Dimarco, F., Wegiel, L., Ferris, S., Kessler, W., Pikal, M., Sacha, G., Alexeenko, A., Thompson, T.N., Reiter, C., Searles, J., Coiteux, P., 2017. Recommended best practices for process monitoring instrumentation in pharmaceutical freeze-drying—2017. AAPS Pharm. Sci. Tech. 18(7), 2379-2393. https://doi.org/10.1208/s12249-017-0733-1

Nakagawa, K., Hottot, A., Vessot, S., Andrieu J., 2007. Modeling of freezing step during freeze-drying of drugs in vials. AIChE J. 53(5), 1362-1372. https://doi.org/10.1002/aic.11147

Napoletano, F., 2016. Mathematical modeling of the freezing process for parenteral products, Tesi di Laurea Magistrale, Politecnico di Torino, Italy.

Oetjen, G.W., Haseley P., 2004. Freeze-drying, 2nd edition, Wiley-VHC, Weinheim.

Oddone, I., Barresi, A.A., Pisano, R., 2017. Influence of controlled ice nucleation on the freeze-drying of pharmaceuticals products: The secondary drying step. Int. J. Pharm. 524(1-2), 134-140. https://10.1016/j.ijpharm.2017.03.077

Parvis, M., Grassini, S., Barresi, A.A., 2012. Sputtered thermocouple for lyophilization monitoring. Proceedings of IEEE International Instrumentation and Measurement Technology Conference (I2MTC), Graz, Austria, May 13–16, 1994-1998. https://doi.org/10.1109/I2MTC.2012.6229263

Parvis, M., Grassini, S., Fulginiti, D., Pisano, R., Barresi, A.A., 2014. Sputtered thermocouple array for vial temperature mapping. Proceedings of IEEE International Instrumentation and Measurements Technology Conference (I2MTC), Montevideo, Uruguay, Maggio 12–15, 1465-1470. https://doi.org/10.1109/I2MTC.2014.6860988

Patel, S.M., Doen, T., Pikal, M.J., 2010. Determination of end point of primary drying in freeze-drying process control. AAPS PharmSciTech. 11(1), 73-84. https://doi.org/10.1208/s12249-009-9362-7

Pearson, K., 1901. On lines and planes of closest fit to systems of points in space. Philos. Mag. 2(11), 559–572. https://doi.org/10.1080/14786440109462720

Pikal, M.J., 1990a. Freeze-drying of proteins. Part I: process design. Biopharm. 3(8), 18-27.

Pikal M.J., 1990b. Freeze-drying of proteins. Part II: formulation selection. Biopharm. 3(9), 26-30.

Pisano, R., Capozzi, L.C., 2017. Prediction of product morphology of lyophilized drugs in the case of Vacuum Induced Surface Freezing. Chem. Eng. Res. Des. 125, 119-129. https://doi.org/10.1016/j.cherd.2017.07.004

Pisano, R., Fissore, D., Velardi, S.A., Barresi, A.A., 2010. In-line optimization and control of an industrial freeze-drying process for pharmaceuticals. J. Pharm. Sci. 99(11), 4691-4709. https://doi.org/10.1002/jps.22166

Pisano, R., Fissore, D., Barresi, A.A., 2011a. Freeze-drying cycle optimization using Model Predictive Control techniques. Ind. Eng. Chem. Res. 50(12), 7363-7379. https://doi.org/10.1021/ie101955a

Pisano, R., Fissore, D., Barresi, A.A., 2011b. Heat transfer in freeze-drying apparatus, in dos Santos Bernardes, M. A. (Ed.), Developments in Heat Transfer, Chapter 6, 91-114. InTech, Rijeka (Croatia). https://doi.org/10.5772/23799

Pisano, R., Barresi, A.A., Capozzi, L.C., Novajra, G., Oddone, I., Vitale-Brovarone, C., 2017. Characterization of the mass transfer of lyophilized products based on X-ray micro-computed tomography images. Drying Technol. 35(8), 933-938. https://doi.org/10.1080/07373937.2016.1222540

Prats-Montalbán, J.M., De Juan, A., Ferrer, A., 2011. Multivariate image analysis: a review with applications. Chemom. Intell. Lab. Syst. 107, 1-23. https://doi.org/10.1016/j.chemolab.2011.03.002

Rambhatla, S., Ramot, R., Bhugra, C., Pikal M.J., 2004. Heat and mass transfer scale-up issues during freeze drying: II. Control and characterization of the degree of supercooling. AAPS PharmSciTech, 5(4), 54-62. https://doi.org/10.1208/pt050458

Reid, D.S., 1984. Cryomicroscope studies of the freezing of model solutions of cryobiological interest. Cryobiol. 21(1), 60–67. https://doi.org/10.1016/0011-2240(84)90023-3

Schneid, S., Gieseler H., 2008. Evaluation of a new wireless temperature remote interrogation system (TEMPRIS) to measure product temperature during freeze-drying. AAPS PharmSciTech 9(3), 729–739. https://doi.org/10.1208/s12249-008-9099-8

Searles, J., Carpenter, J., Randolph T., 2001. The ice nucleation temperature determines the primary drying rate of lyophilization for samples frozen on a temperature-controlled shelf. J. Pharm. Sci. 90(7), 860-871. https://doi.org/10.1002/jps.1039

Van Bockstal, P.J., Corver, J., De Meyer, L., Vervaet, C., De Beer, T., 2018. Thermal imaging as a

noncontact inline process analytical tool for product temperature monitoring during continuous freeze-drying of unit doses. Anal. Chem. 90(22), 13591-13599. https://doi.org/10.1021/acs.analchem.8b03788

Velardi, S.A., Barresi, A.A., 2008. Development of simplified models for the freeze-drying process and investigation of the optimal operating conditions. Chem. Eng. Res. Des. 87(1), 9-22. https://doi.org/10.1016/j.cherd.2007.10.007

Woinet, B., Andrieu, J., Laurent, M., Min, S.G., 1998. Experimental and theoretical study of model food freezing. Part II. Characterization and modelling of the ice crystal size. J. Food. Eng 35(4), 395–407. https://doi.org/10.1016/S0260-8774(98)00036-3

List of Figures

bars represent one standard deviation of variability of d_p.

Figure 6. Values of ice crystal diameters as a function of the frozen layer thickness as predicted by model #1 (graph A) and by model #2 (graph B) for the case of the 5% w/w mannitol solution. Error bars represent one standard deviation of variability of d_p.

Figure 7. Comparison between the mean values of ice crystal diameters predicted using model #1 (short-dashed lines) and #2 (dashed lines) and values measured through SEM analysis (solid lines) for the 5% w/w sucrose solution (graph A) and for the 10% w/w sucrose solution (graph B). The solid lines report the average crystal pore diameters measured, while the bars represent the 25^{th} and the 75^{th} percentiles of the distributions.

Figure 8. Comparison between the curves of R_p vs. L_{dried} predicted using model #1 (solid lines) or model #2 (dashed lines) for the 5% w/w sucrose solution (graph A) and for the 10% w/w sucrose solution (graph B).

Figure 9. Evolution of the pressure ratio vs. time and of L_{frozen} vs. time, as predicted by the mathematical model using the curve of R_p vs. L_{dried} given by model #1, for the 5% w/w sucrose solution (upper graph) and for the 10% w/w sucrose solution (graph B). In both cases the primary drying stage is carried out at 10 Pa, with a shelf temperature of -20°C.

Figure 10. Evolution of the pressure ratio vs. time and of L_{frozen} vs. time, as predicted by the mathematical model using the curve of R_p vs. L_{dried} given by model #2, for the 5% w/w sucrose solution (upper graph) and for the 10% w/w sucrose solution (graph B). In both cases the primary drying stage is carried out at 10 Pa, with a shelf temperature of -20°C.

Figure 1

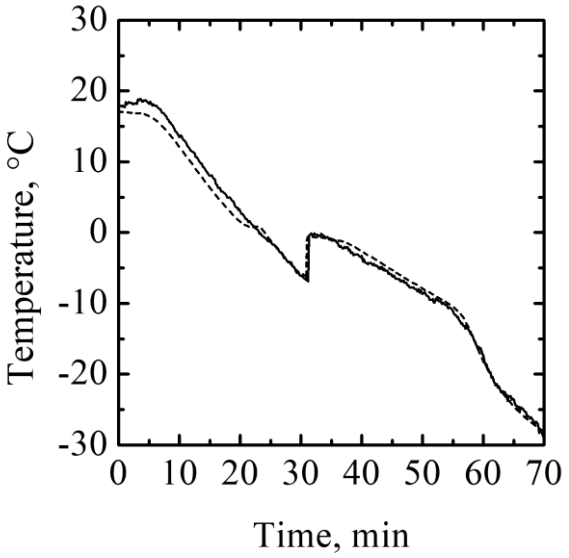

Figure 2

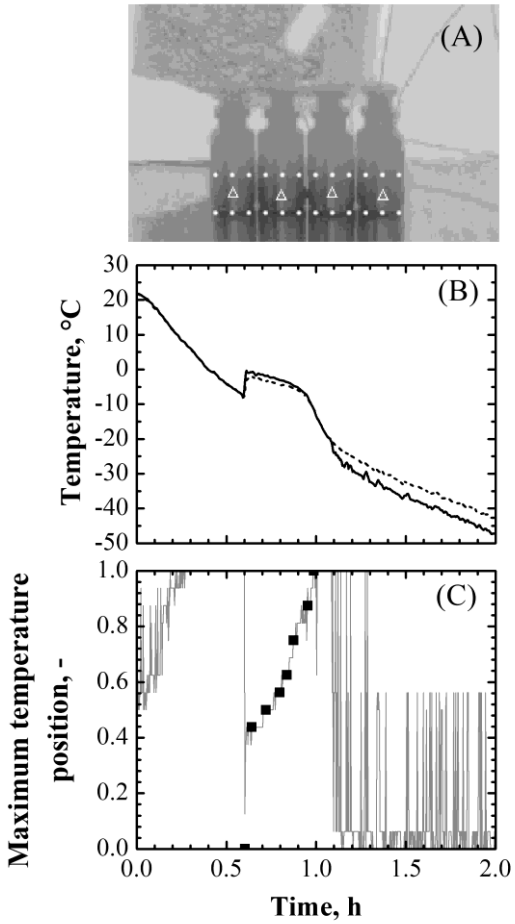
(A)
(B)
(C)
Temperature, °C
30
20
10
0
-10
-20
-30
-40
-50
Maximum temperature position, -
1.0
0.8
0.6
0.4
0.2
0.0
0.0
0.5
1.0
1.5
2.0
Time, h

Figure 3

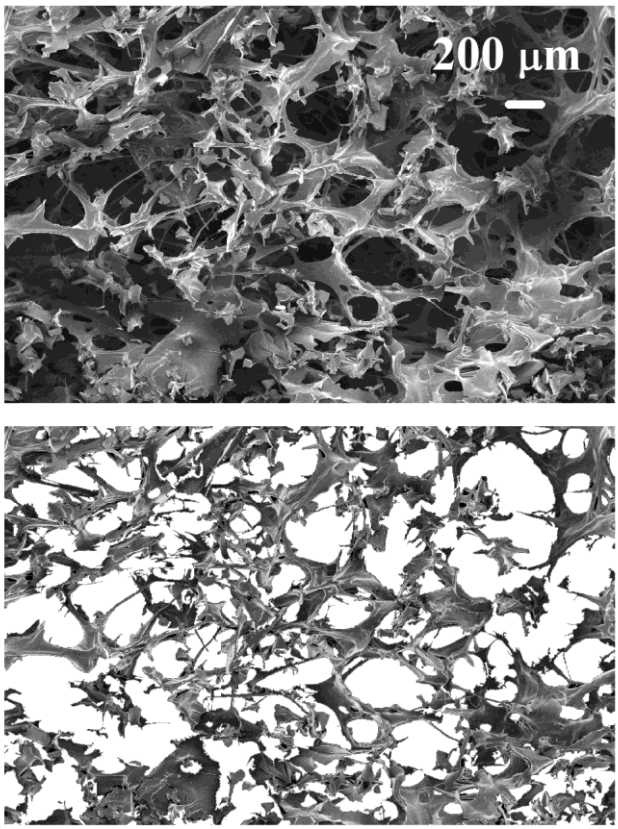

Figure 4

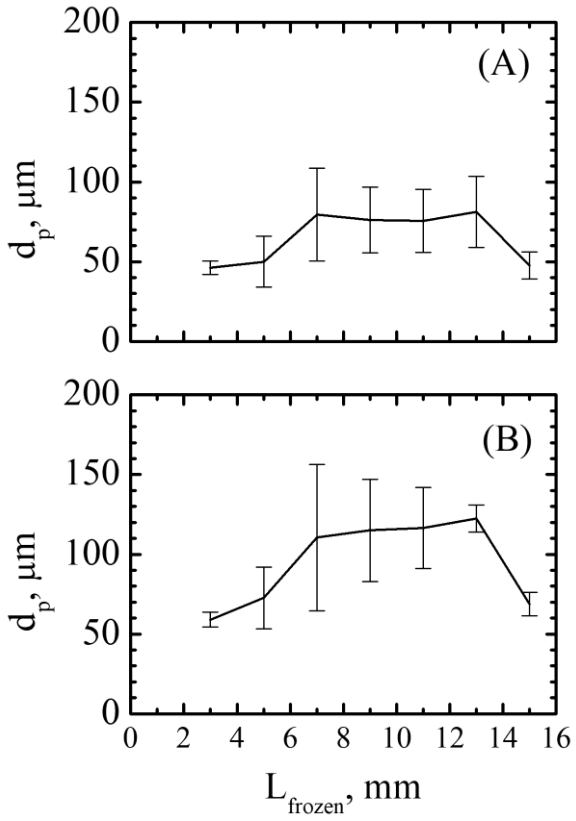

Figure 5

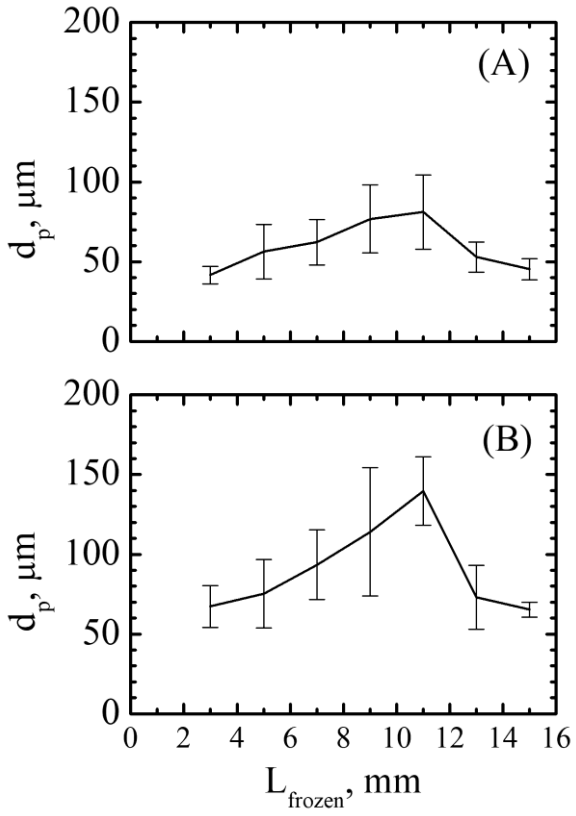

Figure 6

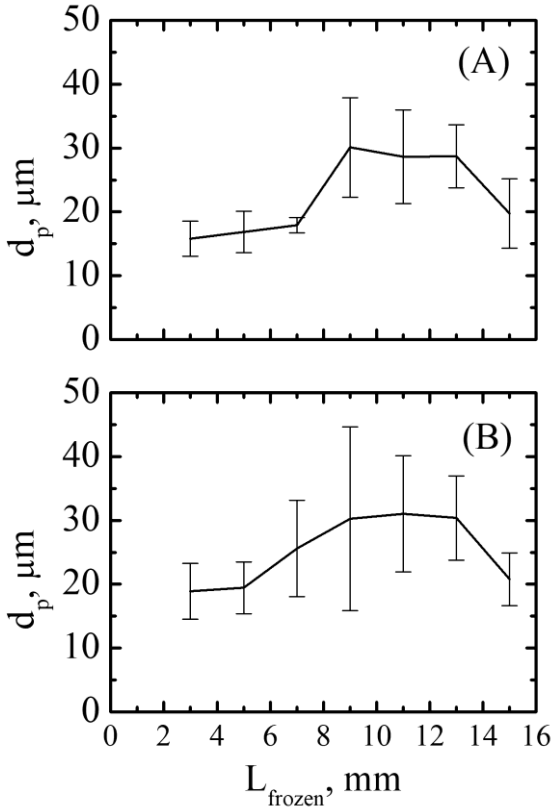

Figure 7

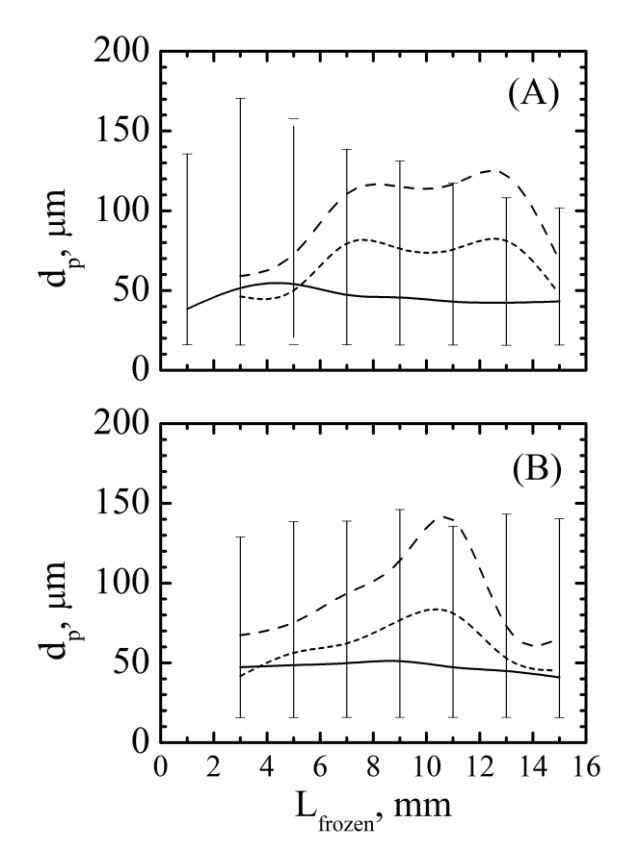

Figure 8

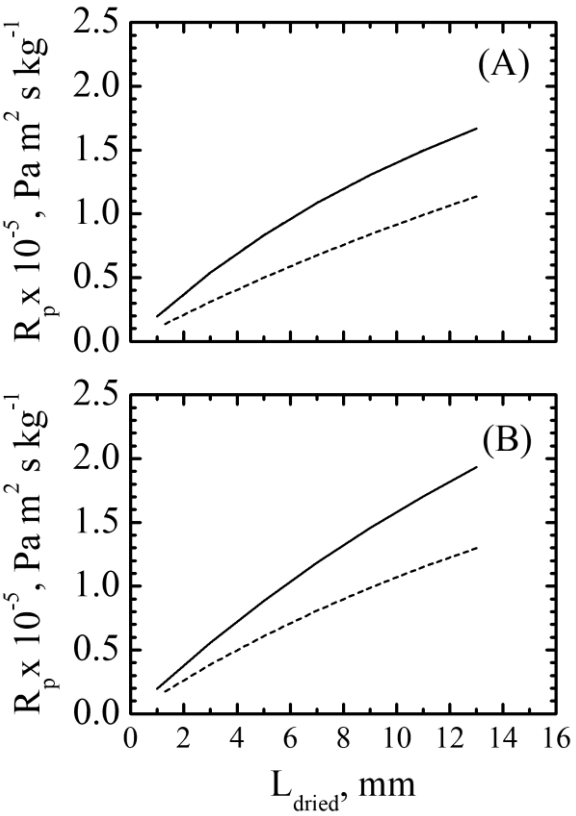

Figure 9

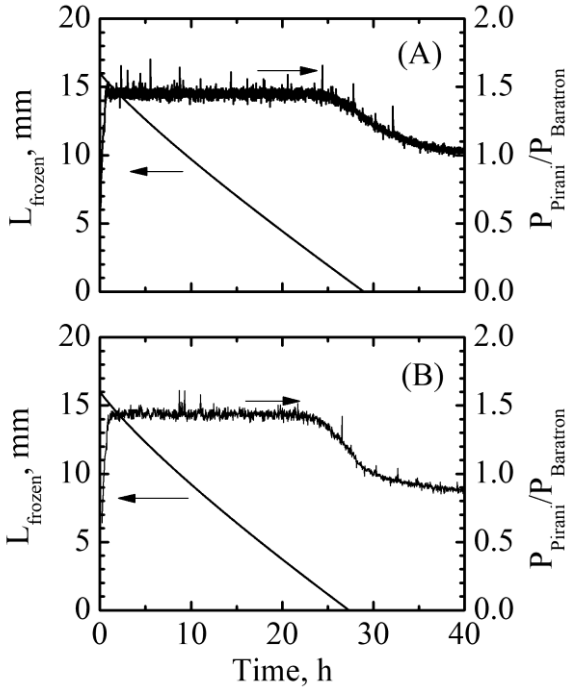
(A)
(B)
L_{frozen}, mm
$P_{Pirani}/P_{Baratron}$
Time, h
0
5
10
15
20
0.0
0.5
1.0
1.5
2.0
0
10
20
30
40

Figure 10

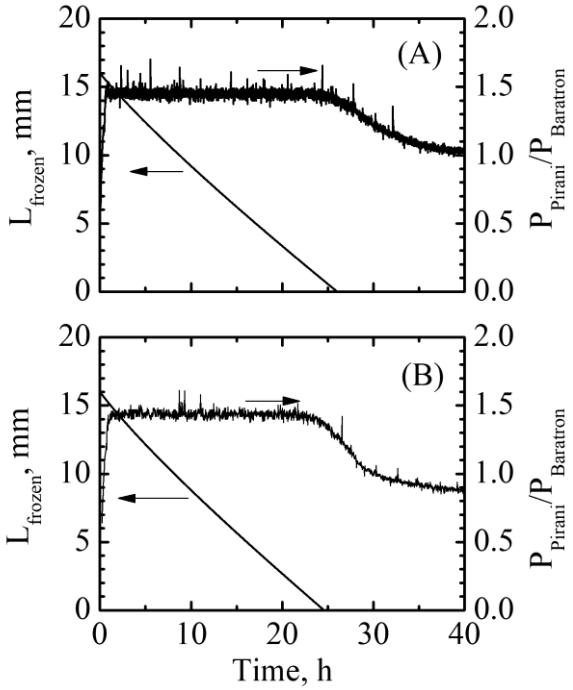
(A)
(B)
L_{frozen}, mm
$P_{Pirani}/P_{Baratron}$
Time, h
0
5
10
15
20
0.0
0.5
1.0
1.5
2.0
0
10
20
30
40